Downloaded from orbit.dtu.dk on: Dec 18, 2017

Technical University of Denmark

Correlation of mesoscale wind speeds over the sea

Mehrens, Anna R.; Hahmann, Andrea N.; Hahmann, Andrea N.; Larsén, Xiaoli Guo; von Bremen, Lueder

Published in:
Quarterly Journal of the Royal Meteorological Society

Link to article, DOI:
10.1002/qj.2900

Publication date:
2016

Document Version
Publisher's PDF, also known as Version of record

Link back to DTU Orbit

Citation (APA):
Mehrens, A. R., Hahmann, A. N., Hahmann, A. N., Larsén, X. G., & von Bremen, L. (2016). Correlation of mesoscale wind speeds over the sea. Quarterly Journal of the Royal Meteorological Society, 142(701 Part B), 3186–3194. DOI: 10.1002/qj.2900

DTU Library
Technical Information Center of Denmark

General rights
Copyright and moral rights for the publications made accessible in the public portal are retained by the authors and/or other copyright owners and it is a condition of accessing publications that users recognise and abide by the legal requirements associated with these rights.

- Users may download and print one copy of any publication from the public portal for the purpose of private study or research.
- You may not further distribute the material or use it for any profit-making activity or commercial gain
- You may freely distribute the URL identifying the publication in the public portal

If you believe that this document breaches copyright please contact us providing details, and we will remove access to the work immediately and investigate your claim.

RMetS
Royal Meteorological Society

Correlation and coherence of mesoscale wind speeds over the sea

Anna R. Mehrens,*[a] Andrea N. Hahmann,[b] Xiaoli G. Larsén[b] and Lueder von Bremen[a]
[a]*Department of Physics, ForWind – Center for Wind Energy Research, Carl von Ossietzky University, Oldenburg, Germany*
[b]*Wind Energy Department, Technical University of Denmark, Roskilde, Denmark*

*Correspondence to: A. R. Mehrens, Department of Physics, ForWind – Center for Wind Energy Research, Carl von Ossietzky University, Oldenburg, Germany. E-mail: anna.mehrens@forwind.de

A large offshore observational dataset from stations across the North and Baltic Seas is used to investigate the planetary boundary-layer wind characteristics and their coherence, correlation and power spectra. The data from thirteen sites, with pairs of sites at horizontal distances of 4 to 848 km, are analyzed for typical wind turbine nacelle heights. Mean wind characteristics, correlation and coherence are also calculated for analogous wind data from simulations with the Weather Research and Forecasting (WRF) model.

Results indicate a general good agreement for the coherence calculated based on measurements and the WRF-derived time series. By normalizing the frequency axes with the distance and mean wind speed, it can be demonstrated that, even for data with a wide range of distances, the coherence is a function of the frequency, mean wind and distance, which is consistent with earlier studies. However the correlation coefficient as a function of distance calculated from WRF is higher than observed in the measurements. For the power spectra, wind speed and wind speed step change distribution, the results for all sites are quite similar. The land masses strongly influence the individual wind direction distribution at each site. The ability of the WRF model to reproduce the coherence of the measurements demonstrates that its output can be used to estimate the coherence of fluctuations for the integration of offshore energy. The power spectra of WRF time series underestimates the high-frequency fluctuations. Due to the large number of measurement sites, the results can be used for further plausibility validation for mesoscale model runs over the sea.

Key Words: coherence; cross-spectrum; power spectrum; offshore; wind integration, wind correlation

Received 3 June 2016; Revised 11 August 2016; Accepted 12 August 2016; Published online in Wiley Online Library 7 October 2016

1. Introduction

The efficient integration of wind energy into the electric transmission grid requires knowledge of wind speed characteristics at the wind farm sites and how their power outputs are correlated. Many offshore wind farms are built over small geographical areas and thus their clusters of wind farms are simultaneously affected by mesoscale wind phenomena. The aggregated power of these offshore wind farms is more fluctuating than for spatially dispersed wind turbines on land (Focken *et al.*, 2002; Akhmatov *et al.*, 2005; Giebel, 2007).

A successful integration not only depends on the mean wind statistics and their correlation, but also on its spectral and cross-spectral properties. For example, the model of Sørensen *et al.* (2002) calculates the power response for several wind farms and is based on their spectral and co-spectral properties.

For the correlation and cross-spectral properties of two measurement sites, different scenarios are possible, depending on the wind direction and the angle of the line connecting the two sites (separation line). If the wind direction is along the separation line of two wind farms (longitudinal), there is a lag between the time when the farms experience a wind speed change. If the distance is large, the change may not be merely advected but may be altered by some meteorological phenomenon which causes the wind characteristics to change. If the flow is perpendicular to the separation line (lateral), there is no time lag between variations at the two sites. However, if the distance between the sites is large, the two sites might not experience the same wind speed change, because the scale of the phenomenon causing the change is smaller than the separation distance.

Several studies have investigated the cross-spectral properties of wind speed measurements with varying measurement distances. Kristensen and Jensen (1979) analysed experimental data laterally separated by a distance of less than 20 m. They presented the normalization of the frequency axis with the distance and mean wind speed, which will be used in this article. Schlez and Infield (1998)

© 2016 The Authors. *Quarterly Journal of the Royal Meteorological Society* published by John Wiley & Sons Ltd on behalf of the Royal Meteorological Society.
This is an open access article under the terms of the Creative Commons Attribution-NonCommercial-NoDerivs License, which permits use and distribution in any medium, provided the original work is properly cited, the use is non-commercial and no modifications or adaptations are made.

investigated longitudinal and lateral coherence for distances of 62–102 m and established an empirical expression for the coherence as a function of mean wind speed, distance and the angle of the separation line. Davenport (1961) examined the coherence of vertically separated observations with a maximum distance of 141 m and expressed the coherence as an exponential function of distance and a reference wind speed. Further analyses of the coherence have been done by Sørensen *et al.* (2002) and Sørensen *et al.* (2008) for a maximum distance of 1.2 km above water and in coastal areas. For flat and complex terrain, the coherence was analysed for distances up to 1.7 km by Nanahara *et al.* (2004). Vigueras-Rodríacuteguez *et al.* (2012) used power measurements at a wind farm with a maximum distance of 7.73 km to develop a coherence model; in our study, this model is used for comparison. The spectral and cross-spectral properties were investigated by Vincent *et al.* (2013) and Larsén *et al.* (2013) for a maximum distance of 12.42 km. Vincent *et al.* (2013) also investigated the wind direction dependency and derived the coherence as a function of frequency, wind speed, distance and the angle of the separation line to the wind direction. Their study showed that the wind simulated by the WRF model reproduces the spatial wind speed coherence for distances up to 12 km and thus can be used to estimate the coherence for regions where no measurements are available. The largest distances investigated by Woods *et al.* (2011) were 30 km.

The aim of our study is to show the main wind speed characteristics for various offshore sites and the correlation and coherence of wind speeds over water in the North and Baltic Seas with larger distances than in existing studies (up to 848 km). Besides the investigation of the coherence, the database will be used to study the mean wind statistics over the North and Baltic Seas to compare the power spectra of the wind speed time series with the analytical model of Larsén *et al.* (2013) for mesoscale winds. The spectral characteristics of wind speed on different scales have been the focus of several studies; Larsén *et al.* (2013) give an overview.

This article focuses on mesoscale winds at a time-scale of several tens of minutes up to several hours. We investigate the spatial coherence of these winds over distances up to 848 km. This scale is especially important for the integration of offshore wind power, because of enhanced mesoscale variability during special weather situations (Vincent *et al.*, 2011), which may simultaneously affect several wind farms. Section 2 presents the database in the North and Baltic Seas. In section 3 the model set-up for the WRF simulation is described, which is used for comparisons. The methodology used is introduced in section 4 and the results are shown and discussed in section 5. The last section 6 concludes our results.

2. Observations

For the calculation of the correlation and coherence, pairs of wind speed measurements with distances between 4 and 848 km are used. The locations of the met masts and lidars are shown in Figure 1(a), together with the corresponding distances in Figure 1(b). The measurement sites are located offshore, near the shore and one is onshore, but very close to the coastline. Depending on the site and wind direction, the wind characteristics are influenced by different roughness lengths, land–sea transitions and the existence of other wind farms. For all sites one height is chosen which is close to a typical offshore nacelle height, but free from wakes of the measuring

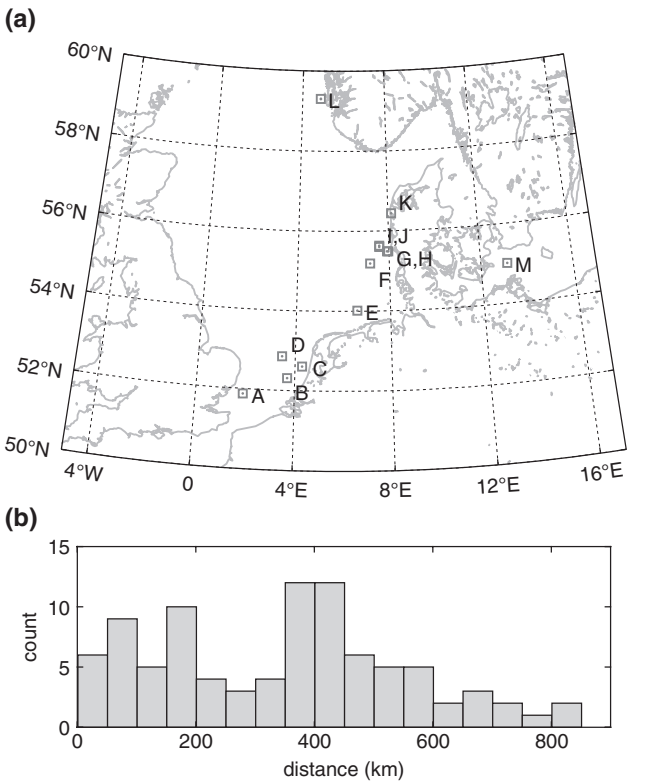

Figure 1. (a) Measurement sites in the North and Baltic Seas and (b) a histogram showing the distances between each pair of sites.

platform (Peña *et al.*, 2012). If measurements at different heights are available, a measurement height was used for which mean wind speed and wind rose are consistent with measurements at other heights. The measurement height, measurement type and the amount of missing values at each site are shown in Table 1. Most time series have around 10% of missing values, with lidar measurements having the highest percentage. All time series are checked for plausibility. For the met masts, where wind speed measurements for more than one boom direction are available, the wind speed is combined depending on the wind direction measurements to exclude mast shadow measurements. Due to confidentiality agreements, the measurement sites are not named, but labelled with letters A to M in Table 1 and the following figures.

All time series consist of 10 min average data and are longer than one year to represent all seasons. However, the individual time series can represent different years and the overlapping time is for some site combinations shorter than a year and thus not representative for all seasons. The availability of data at the different sites is shown in Figure 2.

Wake situations and flow from land are not excluded, since most of the data would be discarded in these cases. According to Sørensen *et al.* (2008), Troldborg *et al.* (2011), Vincent *et al.* (2013) and Larsén *et al.* (2013) mesoscale frequencies are not influenced by wind farm wakes in 10 min time series.

3. Mesoscale simulations

We use data from a numerical simulation for the North and Baltic Seas (region shown in Figure 3) conducted with the

Table 1. Measurement heights, types for all the used measurement sites and the percentage of missing values (NaN).

Site	A	B	C	D	E	F	G	H	I	J	K	L	M
Height (m)	82	90	116	92	90	90	70	70	126	97	100	100	92
Device*	m	l	m	m	m	m	m	m	l	m	m	l	m
NaN (%)	22	17	11	3	5	10	10	5	18	8	7	44	24

* 'l' denotes a WindCUBE lidar measurement and 'm' a met mast measurement.

© 2016 The Authors. *Quarterly Journal of the Royal Meteorological Society* published by John Wiley & Sons Ltd on behalf of the Royal Meteorological Society.

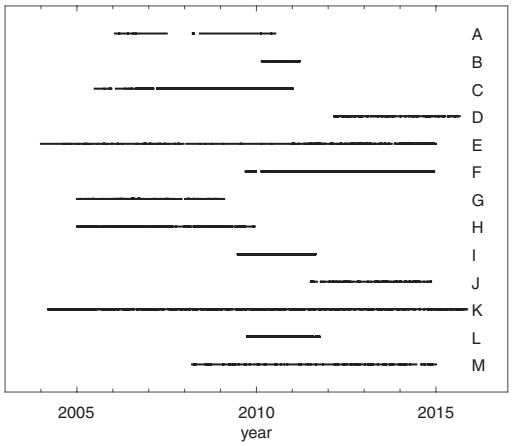

Figure 2. Temporal availability of the measurement sites.

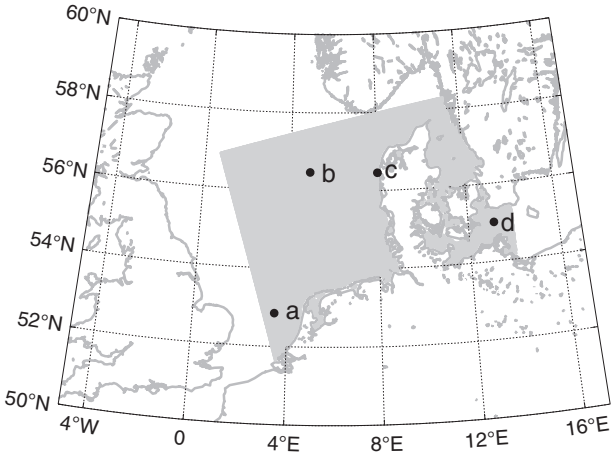

Figure 3. Area of the WRF simulations in the North and Baltic Seas; the marked locations were used to calculate the correlation and coherence.

Advanced Research Weather Research and Forecasting Model (WRF) version 3.5.1. The simulation follows the set-up in Hahmann *et al.* (2015) but with the parametrizations shown in Table 2.

The simulation uses the data from the European Centre for Medium Range Forecast (ECMWF) ERA-Interim Reanalysis (Dee *et al.*, 2011) with 0.75°grid spacing to initialize, update the boundaries, and for the fields used in the grid nudging. Sea surface temperature (SST) and sea-ice fractions come from the dataset produced at NOAA/NCEP* at 0.25°resolution (Reynolds *et al.*, 2007) and are updated daily. The outer domain has a grid spacing of 18 km. Two other domains are nested within, with grid spacings of 6 and 2 km on a polar stereographic projection. The simulations use 41 vertical levels from the surface to a height of approximately 20 km. The levels are closer together near the Earth's surface to better simulate the processes occurring in the planetary boundary layer (PBL). The lowest ten of these levels are within 1000 m of the surface and the first level is located at approximately 14 m above mean sea level. The simulation ran in a series of 11-day long overlapping simulations, with the output from the first day being discarded to allow the model to spin up. The simulation used spectral nudging which continuously relaxes the model solution towards the gridded reanalysis, but this is done only on the outer domain and above level 10 to allow for the mesoscale processes near the surface to develop freely. This method is based on the assumptions described in Hahmann *et al.* (2010) and validated in Hahmann *et al.* (2015) for wind energy applications offshore in the Baltic and North Seas. The grid nudging and 10-day reinitialization keeps the model solution from drifting from the observed large-scale atmospheric patterns, while the relatively long simulations guarantee that the mesoscale flow is fully in equilibrium with the mesoscale characteristics of the terrain.

*(USA) National Oceanic and Atmospheric Administration/ National Centers for Environmental Prediction.

Table 2. Parametrizations used in the WRF model simulations.

Parameter	Setting
Short-wave radiation	Dudhia (option 1)
Long-wave radiation	RRTM (option 1)
Precipitation	WRF single-moment 5-class (option 4) and Kain–Fritsch (option 1), turned off on outer domain.
PBL and land surface	Yonsei University (option 1), MM5 similarity (option 1) and Noah Land Surface Model (option 2)

One major difference from the standard WRF modelling system is the change in land use and its associated surface roughness length. Detailed inspection of the standard land use maps in WRF showed serious problems. For the simulation, an averaged land use map for the period 2001–2010 derived from MODIS Collection 5 (Friedl *et al.*, 2010) is used, as opposed to the MODIS C4-based data from a single year for 2001 used in the default WRF v 3.5.1. Surface roughnesses were modified to better represent the characteristics of the terrain in this region. In addition to the new values, the annual variation in surface roughness used in WRF was disabled because of the unrepresentative spatial and temporal resolution of the driving fractional vegetation cover.

This study includes the data for the period 2000–2013 at a height of around 100 m (level 4) with a temporal resolution of 10 min for the wind speed and 1 h for the wind direction. For the analysis presented here, we use only a part of the inner domain (the area we are interested in), with grid points which are at least 2 km away from land.

4. Methodology

The wind speed characteristics of each site are shown by the frequency distribution of the wind speed and wind speed step changes. For better comparison of the wind speed distribution, the wind speed is normalized by the mean wind speed at each site. The frequency distribution of wind speed step changes (δu) shows the occurrence of wind speed changes within two consecutive time steps (i and $i+1$):

$$\delta u = u_{i+1} - u_i \,. \tag{1}$$

To interpret the wind direction distribution at different sites, wind roses are compared.

The power spectra of each site have been calculated for the whole wind speed time series, using the Fast Fourier Transform. Missing values are filled by linear interpolation between the last and first available value around the data gap.

For the comparison of the correlation of different measurement site combinations for all overlapping time series, the Pearson correlation coefficient is calculated without shifting the time series (xlag = 0):

$$\rho(A,B) = \frac{\mathrm{cov}(A,B)}{\sigma_A \sigma_B}, \tag{2}$$

with the covariance (cov) and the standard deviation (σ) of the sites A and B.

The correlation coefficient is calculated for different time averages, representative not only of the mesoscale, but also the synoptic scale. To compare the correlation coefficient of different distances between measurements and WRF simulation

© 2016 The Authors. *Quarterly Journal of the Royal Meteorological Society* published by John Wiley & Sons Ltd on behalf of the Royal Meteorological Society.

grid points, four grid points in the model area are chosen (Figure 3(a)–(d)). The correlation coefficient is calculated for these individual four points with all other grid points. These four points were chosen because of their varied distances to the coast and proximity to the observational sites (section 3).

For the cross-spectral properties, the coherence (Coh) is calculated:

$$\mathrm{Coh}(f) = Co_n(f) + \mathrm{i}\, Qu_n(f), \tag{3}$$

where f is the frequency.

It consists of the cospectrum (Co_{AB}) and the quadrature spectrum (Qu_{AB}) of the two sites A and B:

$$Co_n(f) = \frac{\overline{Co_{AB}}(f)}{\sqrt{\overline{P_A(f)P_B(f)}}}, \tag{4}$$

$$Qu_n(f) = \frac{\overline{Qu_{AB}}(f)}{\sqrt{\overline{P_A(f)P_B(f)}}}, \tag{5}$$

normalized with the power spectra of the two time series (P_A and P_B). The spectral energy P is obtained using the Welch's power spectral density estimate with a Hanning window. The cospectrum represents the *in-phase* fluctuations and the quadrature spectrum the *out of phase* fluctuations. Due to the normalization with the power spectra, a perfect correlation for a certain frequency is reached when the coherence is equal to 1.

Whether the two time series have a negative or positive quadrature spectrum depends on the definition of the angle of the separation line to the main wind direction. The separation line is always defined for positive quadrature spectra.

For the investigated measurement site distances, the entire time series can hardly be regarded as stationary to fulfill the requirements for the Fast Fourier Transform. Thus, the coherence is calculated for each day individually and the following criteria have to be fulfilled by both time series to reach near-stationarity: the difference between minimum and maximum wind speed during one day is $\leq 12\,\mathrm{m\,s^{-1}}$ and in wind direction is $\leq 90^\circ$. Afterwards, each day time series is linearly detrended. Due to this procedure, several days of the investigated data are rejected and the time overlay of the site combinations gets smaller.

Because of the loss of energy due to missing value interpolation (section 5.4), only days with less than seven missing values out of the 144 are used. The missing values are filled by linear interpolation. As in the correlation calculation, no time series lag adjustment is done. This procedure is similar to the methodology of Vincent *et al.* (2013). They additionally used wind speed and wind direction criteria for the difference of the two masts to ensure that the mean wind speed of both can be regarded as the advection wind speed. Due to the large distances considered in this study, it is questionable whether such an advection wind speed exists. Thus, no criterion is used when comparing the two time series. Nevertheless, the normalization of the frequency axis is done as in Vincent *et al.* (2013) to test if all spectra still collapse to one curve. Due to the requirements for near-stationarity and the limit for missing values in the time series, many days have to be rejected. For the further analysis, measurement site combinations are used, resulting in more than 50 days to analyse. The total available near-stationary days for all possible site combinations are presented in Figure 4. In section 5.6 the mean coherence of all available days is analysed.

No analyses of the influence of the angle between the separation line and the wind direction on the coherence has been done. Because of the large distances between measurement sites, the Coriolis force is no longer negligible and a reference wind direction or advection wind speed is hard to define without requiring the same wind direction at both sites.

For the comparison of the coherence of the measurements with the coherence at different distances in the WRF simulations, the grid point b in the model area is chosen (Figure 3). Similar results are found at other points. Due to high computational costs, only one point was chosen. Point b is used for this study because of its free flow position.

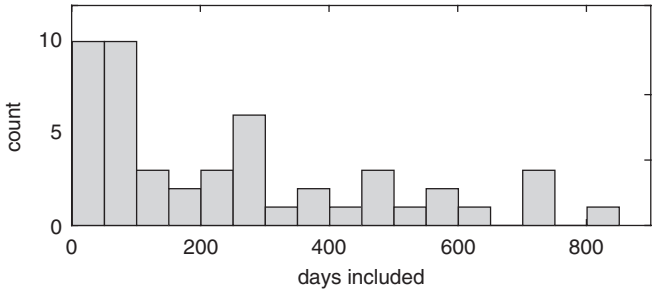

Figure 4. Number of near-stationary days for all possible site combinations. The ten combinations with less than 50 days are rejected from further analysis.

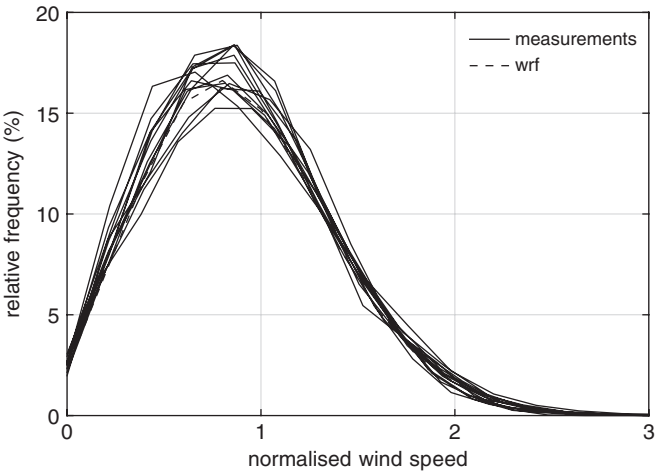

Figure 5. Wind speed frequency distribution for all sites and for point b of the WRF simulation. The x-axis is normalized with the mean wind speed of each individual site.

5. Results and discussion

5.1. Wind speed distribution

The normalized wind speed distributions of all measurement sites and the data of point b of the WRF simulation are shown in Figure 5. Even though the measurement sites are spread over a large area with varying distances to the coastline, the shapes of the distributions are very similar. The distributions widths are site dependent and thus the maximum relative frequency varies within 4%. The results for the WRF simulation data show no distinct deviation from the measurements.

5.2. Probability distribution of wind speed step changes

The probability distribution for the wind speed step changes are shown in Figure 6. The comparison with the fitted Gaussian distribution, which is manually fitted to the maximum values, demonstrates that wind speed step changes do not follow a Gaussian distribution. Wind speed step changes greater than $1\,\mathrm{m\,s^{-1}}$ have a higher probability than they would have if the step changes were normally distributed. This result is comparable to the results of Dowds *et al.* (2015) with the same temporal resolution. Results of Anvari *et al.* (2016) for high-resolution wind and solar power data show the same characteristics. Furthermore, they conclude that the probability for large step changes is lower in wind parks due to smoothing effects.

Figure 6 also compares the probability distribution of the wind speed step changes at the measurement sites with the data at

© 2016 The Authors. *Quarterly Journal of the Royal Meteorological Society* published by John Wiley & Sons Ltd on behalf of the Royal Meteorological Society.

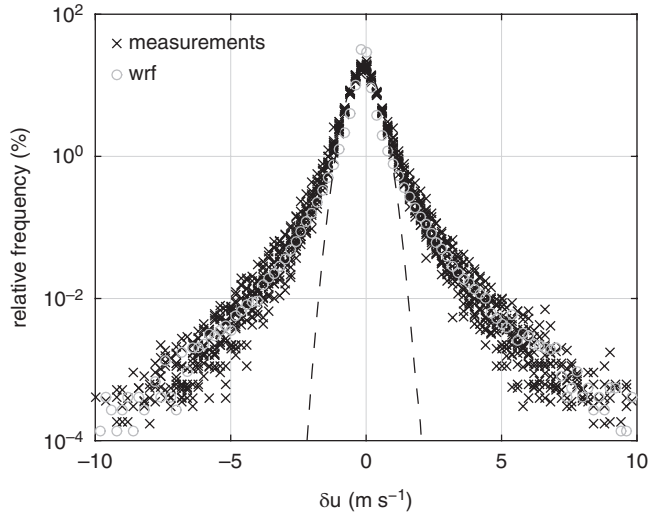

Figure 6. Probability distribution of wind speed changes (δu) within two subsequent 10 min time steps for all measurement sites (crosses) and point b of the WRF simulation (circles) in comparison with a Gaussian distribution (dashed).

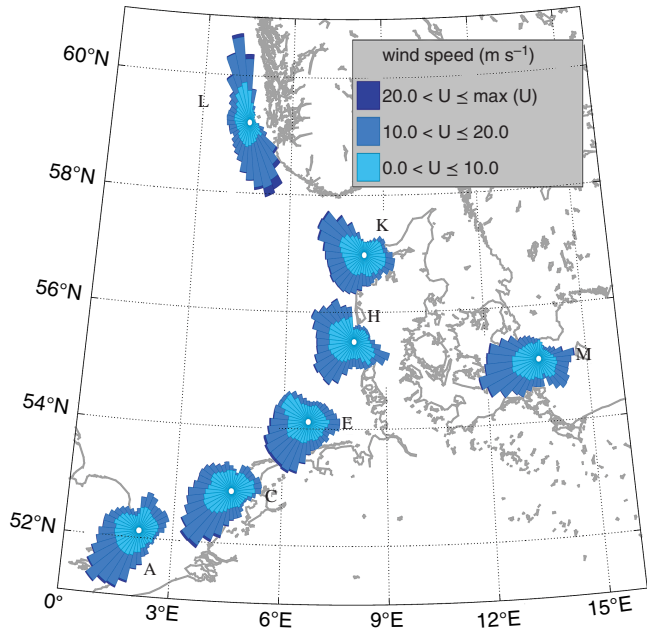

Figure 7. Wind roses for some representative measurement sites. For better visualisation, some roses are slightly shifted from their real measurement locations (see Figure 1).

point b of the WRF simulation. The probability of very small step changes is slightly higher for the WRF simulation data than for the measurements.

5.3. *Wind direction distribution*

Figure 7 shows the wind roses for some representative measurement sites. It can be concluded that the wind direction is more site dependent than the wind speed distribution. The relation to land has a strong impact on the prevailing wind direction. The measurement site A shows a main wind direction from southwest and a second maximum from the northeast. This main wind direction is less pronounced and broader for site E. Site L shows a strong influence of the Norwegian Mountains. The only measurement site in the Baltic Sea (M) has prevailing westerly winds with a second maximum for easterly winds, i.e. different from the main directions in the North Sea.

5.4. *Power spectra*

Figure 8 shows the power spectra from all 13 sites, the analytical model of Larsén *et al.* (2013) for the mesoscale, and one time series derived from the WRF simulations at point b (Figure 3). All spectra are slightly smoothed by calculating the mean value of the energy using log-spaced bins. The model of Larsén *et al.* (2013):

$$S(f) = a_1 f^{-5/3} + a_2 f^{-3}, \tag{6}$$

with $a_1 = 3\times10^{-4}\,\mathrm{m^2\,s^{-8/3}}$ and $a_2 = 3\times10^{-11}\mathrm{m^2\,s^{-4}}$ is based on measurements from two offshore sites, Horns Rev and Nysted, which are included in this study. Figure 8 makes it evident that the analytical model is valid for all investigated measurement sites.

Figure 8 demonstrates that all time series have a peak in the spectral power at a cycle duration of one year. A broader local maxima is located at around 3 days due to synoptic-scale fluctuations in this region. No local maxima for a cycle duration of one day is found, thus none of the offshore sites has a dominant daily cycle at the investigated height. For frequencies higher than the synoptic scale, power spectra for all sites are very similar and larger than the analytical model. For a cycle duration of several hours, the differences in the power spectra increase. Figure 8 also shows the mean wind speed at the different sites. It can be concluded that the mean wind speed at the site has no clear systematic influence on the power spectra of the investigated sites. However, the range of mean wind speeds at the investigated sites is rather limited.

Figure 9 shows the same as Figure 8, but the percentage of missing values of the time series is colour coded. Because of

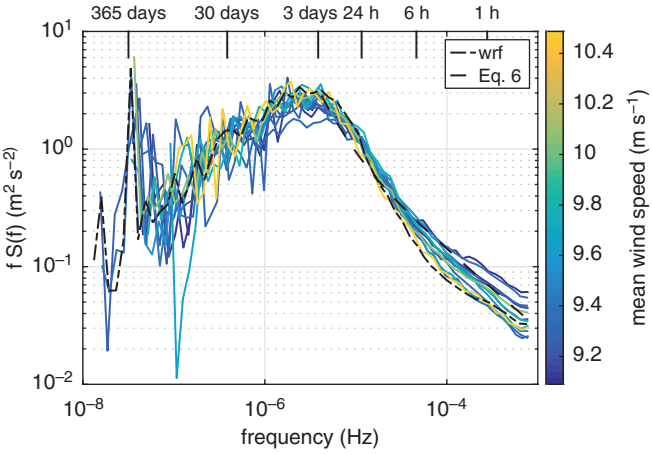

Figure 8. Power spectra for all sites. The dashed lines represent the analytical model of Larsén *et al.* (2013) and the power spectra for the point b of the WRF simulation. The colour code represents the dependency on the mean wind speed of the measurement site.

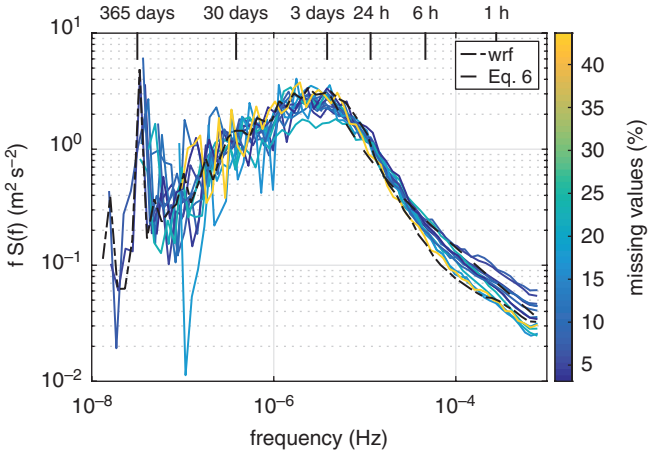

Figure 9. As Figure 8, but here the colour code represents the dependency on the amount of missing values in the analysed time series.

© 2016 The Authors. *Quarterly Journal of the Royal Meteorological Society* published by John Wiley & Sons Ltd on behalf of the Royal Meteorological Society.

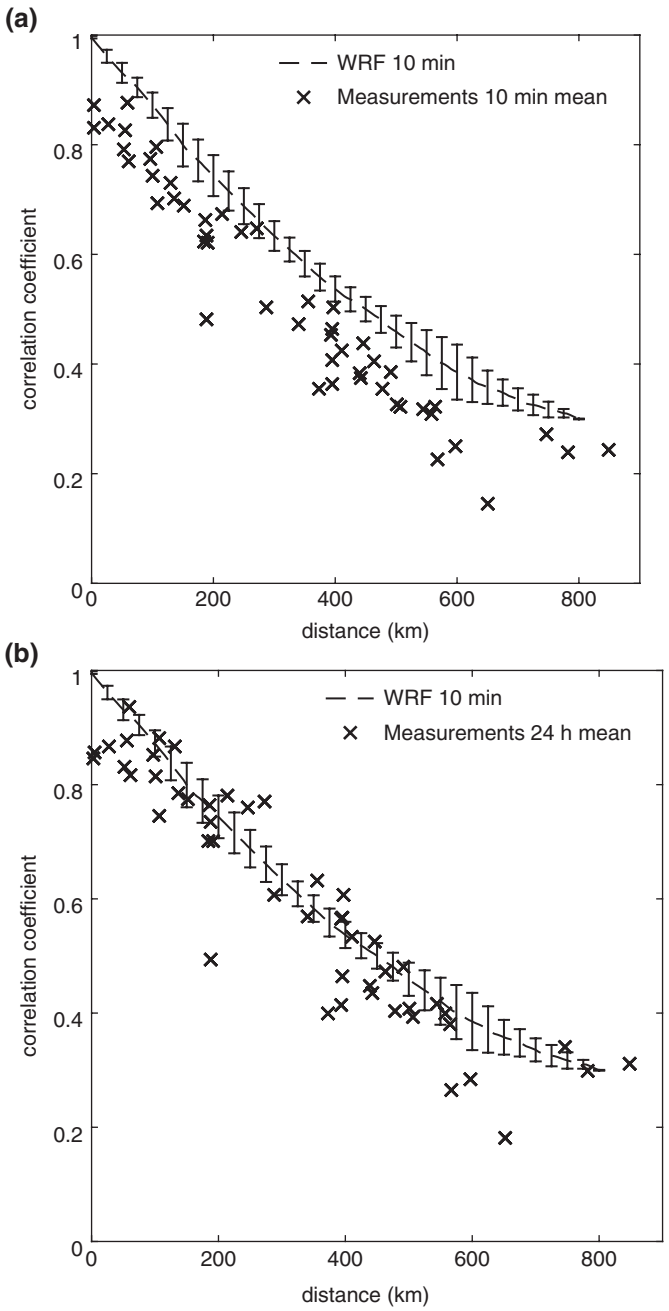

Figure 10. Correlation coefficient for all 10 min mean measurement site combinations (crosses) and the mean of all correlation coefficients for all possible combinations of the four chosen grid points with all other grid points of the WRF simulation. The whiskers show the standard deviation of the WRF-based results. (b) is as (a), but for 24 h mean measurements.

the linear interpolation of the missing values, the time series lose energy at the higher frequencies. The higher the percentage of missing values, the higher the energy loss. This dependency on the percentage of missing values is more pronounced than the dependency on the mean wind speed at the site, colour coded in Figure 8. The comparison of the spectra from the measured data with the WRF data suggested that WRF misses some high-frequency fluctuations, similar to measured time series with a considerable amount of missing data. Larsén *et al.* (2013) states that in the mesoscale range the spectra for the offshore measurement site Horns Rev shows negligible height dependency between 15 and 62 m, because the impact of surface fluxes is already insignificant for this height. There is a chance that the small deviations in the spectra shown are not due to the different heights of the measurements, but more likely depend on the amount and the distribution of missing values in the time series.

5.5. Correlation

The dependency of the correlation coefficient on the distance between all measurement sites is demonstrated in Figure 10(a). The correlation coefficient decreases exponentially with distance. For distances greater than 600 km, the lowest values for the coefficient are reached and for longer distances, up to 840 km, the coefficient approaches a constant value. However, the correlation coefficient does not reach zero, probably because of the impact of the annual cycle.

St. Martin *et al.* (2015) show an overview of publications dealing with the correlation of wind speed and wind power measurements as a function of the measurement site distance. Most publications use an exponential function to describe the decay of the correlation coefficient with distance and agree with our results.

The dashed lines in Figure 10 demonstrate the mean correlation coefficient for the four WRF grid points shown in Figure 3 with all other WRF grid points. The slope of the curve is very similar to the one of the measurements, but is in general shifted to higher values. Figure 10(b) shows the same WRF results as Figure 10(a), but now the measurement correlations are calculated with the daily mean value of the 13 measurement sites. Due to the reduced temporal resolution, the correlation coefficients of the daily averaged measurements are more comparable with the correlations in the WRF data. Even though the results for the WRF simulation data are based on other sites than the measurements including other distances to the coast, the results indicate that WRF is not capable of resolving wind variabilities sufficiently at higher frequencies due to the numerical smoothing. In the measurements these frequencies are included and probably lower the correlation of the measurement points. By removing the high-frequency fluctuations in these measurements by using the daily mean values, measurements and the WRF modelled data achieve better agreement, as shown in Figure 10(b).

This behaviour of WRF, i.e. lack of ability to resolve high-frequency fluctuations, is already visible in Figure 9. The power spectral density of the simulation is lower than the measurements in the mesoscale range. Only the sites with high missing value rates show a similar level of energy. This issue of mesoscale simulations was examined systematically by Skamarock (2004) and Vincent and Hahmann (2015).

5.6. Coherence

Figure 11 shows the normalized amplitude of the coherence for all site combinations which have more than 50 near-stationary days available. All frequencies (f) on the x-axis are normalized with the long-term mean wind speed of both sites (V_o) and the distance (d), as discussed in section 4. The plot suggests that the normalization of the x-axis, which was proved for smaller distances, is still valid. The coherence is still a function of the distance and the wind speed. The results for all possible combinations of measurement sites collapse to a small range (Figure 11), consequently it is reasonable to show only the mean values in Figure 12. A possible explanation for why this normalization is valid for great distances is that these distances are no longer coherent, and so the error introduced by using the mean wind speed as an advection wind speed is negligible.

The coherence is the sum of the cospectrum and the quadrature spectrum (Eq. (3)). The contribution of the quadrature spectrum to the coherence, the out-of-phase fluctuations, is rather small. This is because different angles between the separation line and the wind direction are not investigated separately. This study concentrates on the mean of all near-stationary days. If there is a contribution from the coherence of the out-of-phase fluctuations, the main wind direction of the sites is more often along the separation line than perpendicular to it.

© 2016 The Authors. *Quarterly Journal of the Royal Meteorological Society* published by John Wiley & Sons Ltd on behalf of the Royal Meteorological Society.

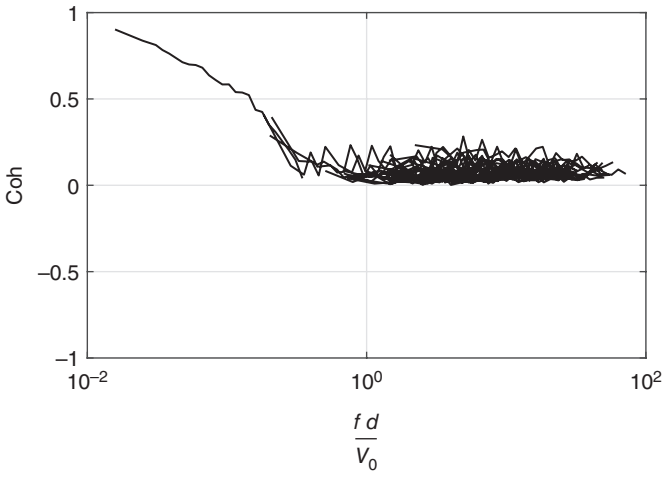

Figure 11. Normalized amplitude of the coherence for all site combinations which have more than 50 near-stationary days available.

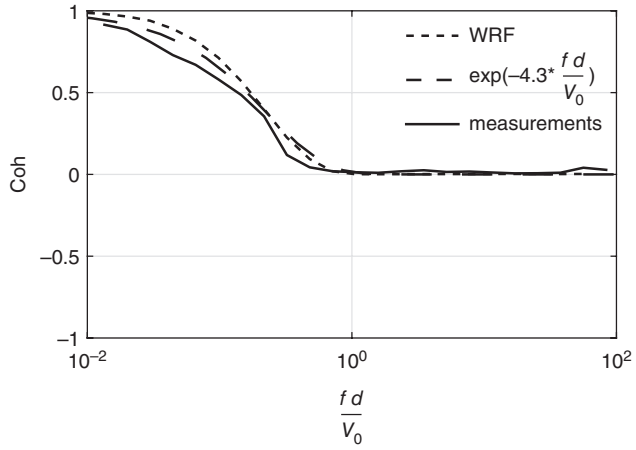

Figure 12. Mean normalized amplitude of the coherence of all measurement sites, WRF simulations and the analytical model of Vigueras-Rodríacuteguez *et al.* (2012).

Figure 12 also compares the mean coherence of all site combinations with the coherence of the wind speed for the point b (Figure 3) in the WRF simulation with all other grid points and the analytical model of Vigueras-Rodríacuteguez *et al.* (2012), based on wind power measurements in a wind farm. In general all three lines show a similar behaviour. The coherence of the data from the WRF simulation has the highest values for low normalized frequencies. This corresponds to the results of section 5.5, where the correlation is larger in the WRF-derived data. The analytical model shows higher values than the measurements in the range of low normalized frequencies. Thus it is closer to the WRF model than to the measurements. However, it must be noted that the low normalized frequency results of the measurements are only based on one measurement (Figure 11), because only one considered measurement site pair has a very small distance.

Due to the normalization of the axis, an understanding of which frequencies f are correlated with which distances d is no longer possible. For the following example in Figure 13, the normalized frequency at which the coherence is 0.1 is used, and thus very little correlation between two time series is left. This point is at a normalized frequency of :

$$\frac{f\,d}{V_0} \approx 0.36 \tag{7}$$

Based on Eq. (7), it is possible to calculate, for each frequency the distance when the coherence is close to zero, depending on the wind speed. Figure 13 shows this dependency for two

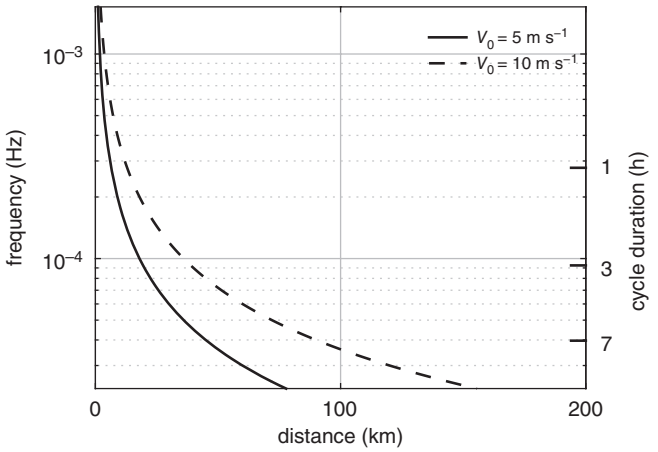

Figure 13. Example for two different wind speeds to illustrate the relation of wind speed, distance and frequency for a coherence of 0.1.

different wind speeds. For lower frequencies the distances for which the coherence is close to zero is greater than that for higher frequencies. With an increase in the wind speed, the distances are greater, up to the frequencies for which different sites are coherent. Because only time series with a maximum length of a day are selected, this is only valid for frequencies in the mesoscale and near-stationary flow.

Due to the high spatial resolution of WRF simulation, the spatial coherence can be analysed and thus the influence of the land masses on the coherence can be examined. Figure 14 shows the coherence of all WRF points with the point b for two frequencies. Figure 14(a) and (b) demonstrate that in general the coherence is lower for greater distances, similar to the results shown earlier. For shorter cycle durations, the decrease is higher.

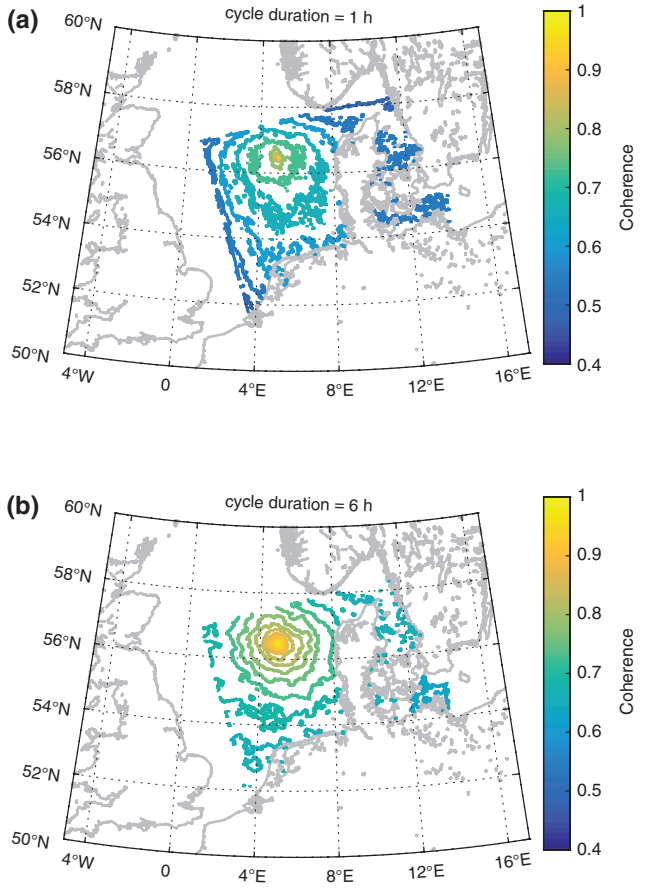

Figure 14. Normalized amplitude of the Coherence for all WRF grid points with the point b for a cycle duration of (a) 1 h and (b) 6 h. Due to the different decrease of the coherence, the contour lines in (a) and (b) do not have the same spacing.

© 2016 The Authors. *Quarterly Journal of the Royal Meteorological Society* published by John Wiley & Sons Ltd on behalf of the Royal Meteorological Society.

In Figure 14(a) the decrease of the coherence above the North Sea is not completely radial. The distance to the coast has a small influence on the decrease of the coherence with distance. Thus, for small cycle durations, the coherence is also a function of the distance to the coast. The reason might be the existence of local wind systems at this time-scale.

6. Summary and conclusions

Coherence, correlation, power spectra and the relative frequency of wind speed, wind speed step change and wind directions were examined for 13 sites over a large water area. Ten-minute data from met mast and lidar measurements in the North and Baltic Seas were used with distances between sites of between 4 and 848 km. Most of the measurement sites are close to the coast. The mean wind characteristics, correlation and coherence were also calculated based on the output from a WRF simulation.

The distribution of wind speeds, wind speed step changes and the power spectra is similar for all sites and the WRF simulation data. Difference in power spectra are likely to appear due to different percentages of missing values which have been interpolated. The dependency on the mean wind speed at the site is less pronounced. The linear interpolation reduces the energy in the time series. It was found that the model of Larsén *et al.* (2013) for the mesoscale power spectra is valid for all sites in this study. The wind roses of the measurements and the spatial plot of the coherence of the WRF simulation indicates that the land masses, and thus distances to the coast, have an influence on the wind speed and wind direction. The correlation as a function of distance can be regarded as an exponential function. For distances greater than 600 km, the correlation stays constant. Even at the maximum distance of 848 km, the correlation coefficient does not reach zero. The correlation coefficient of the WRF data shows the same behaviour, but with higher values. When computing the correlation coefficient with daily mean values of measurements, the correlation is very similar to that of the WRF data. Based on the assumption that the measurements are representative for the WRF domain, this indicates that WRF is not capable of accurately resolving high-frequency or mesoscale wind fluctuations.

The calculation of coherence is extended to distances much larger than shown in previous studies. However, the results are comparable to the older studies like Vincent *et al.* (2013), Vigueras-Rodríacuteguez *et al.* (2012) and Larsén *et al.* (2013). The influence of the angle of the wind direction to the separation line is not investigated here, due to the difficulties in defining one constant wind direction over such a long distance. However, the results confirm that the coherence is a function of the frequency, distance and advection wind speed. Also the model of Vigueras-Rodríacuteguez *et al.* (2012), which was based on measurements within one wind farm, is consistent with our measurements with greater distances. The coherence values of the Vigueras-Rodríacuteguez *et al.* (2012) model are slightly higher than those of the measurements. The coherence in the WRF simulation is even higher than that of the Vigueras-Rodríacuteguez *et al.* (2012) model for small frequencies.

The large number of measurement sites extending over more than 800 km over water is valuable for validating mean wind statistics and spectral properties of mesoscale models.

Acknowledgements

The DAAD is thanked for granting Anna R. Mehrens a three-month stay at the Wind Energy Department, Technical University of Denmark, Roskilde, Denmark. The work presented in this study is funded by the Ministry of Science and Culture of Lower Saxony within the PhD Programme 'System Integration of Renewable Energies' (SEE) and the project 'Ventus efficiens' (ZN3024, MWK Hannover). The authors are grateful to the EU-NORSEWInD project (funding TREN-FP7EN-219048) in collaboration with DONG energy, Statoil Hydro ASA, TAQA, Shell UK, Talisman Energy, Kindle Energy, Scottish Enterprise, Scottish and Southern Renewables, SSE and 3E. The authors acknowledge Vattenfall, Federal Maritime And Hydrographic Agency (BSH) and ECN Wind Energy for providing analysis data. X. G. Larsén acknowledges DONG Energy for access to Horns Rev data through Danish ForskEL project XWiWA (PSO12020). We thank Claire Louise Vincent and Poul Ejnar Sørensen for discussions and suggestions.

References

Anvari M, Lohmann G, Wächter M, Milan P, Lorenz E, Heinemann D, Rahimi Tabar MR, Peinke J. 2016. Short-term fluctuations of wind and solar power systems. *New J. Phys.* **18**: 063027, doi: 10.1088/1367-2630/18/6/063027.

Akhmatov V, Abildgaard H, Pedersen J, Eriksen PB. 2005. 'Integration of offshore wind power into the western Danish power system'. In *Proceedings of the Offshore Wind*. Copenhagen.

Davenport AG. 1961. The spectrum of horizontal gustiness near the ground in high winds. *Q. J. R. Meteorol. Soc.* **87**: 194–211, doi: 10.1002/qj.49708837618.

Dee DP, Uppala SM, Simmons AJ, Berrisford P, Poli P, Kobayashi S, Andrae U, Balmaseda MA, Balsamo G, Bauer P, Bechtold P, Beljaars ACM, van de Berg L, Bidlot J, Bormann N, Delsol C, Dragani R, Fuentes M, Geer AJ, Haimberger L, Healy SB, Hersbach H, Hólm EV, Isaksen L, Kållberg P, Köhler M, Matricardi M, McNally AP, Monge-Sanz BM, Morcrette J-J, Park B-K, Peubey C, de Rosnay P, Tavolato C, Thépaut JN, Vitart F. 2011. The ERA-Interim reanalysis: Configuration and performance of the data assimilation system. *Q. J. R. Meteorol. Soc.* **137**: 553–597, doi: 10.1002/qj.828.

Dowds J, Hines P, Ryan T, Buchanan W, Kirby E, Apt J, Jaramillo P. 2015. A review of large-scale wind integration studies. *Renew. Sustain. Energy Rev.* **49**: 768–794, doi: 10.1016/j.rser.2015.04.134.

Focken U, Lange M, Mönnich K, Waldl HP, Beyer HG, Luig A. 2002. Short-term prediction of the aggregated power output of wind farms – A statistical analysis of the reduction of the prediction error by spatial smoothing effects. *J. Wind Eng. Ind. Aerodyn.* **90**: 231–246, doi: 10.1016/S0167-6105(01)00222-7.

Friedl MA, Sulla-Menashe D, Tan B, Schneider A, Ramankutty N, Sibley A, Huang X. 2010. MODIS collection 5 global land cover: Algorithm refinements and characterization of new datasets. *Remote Sens. Environ.* **114**: 168–182, doi: 10.1016/j.rse.2009.08.016.

Giebel G. 2007. A variance analysis of the capacity displaced by wind energy in Europe. *Wind Energy* **10**: 67–79, doi: 10.1002/we.208.

Hahmann AN, Rostkier-Edelstein D, Warner TT, Vandenberghe F, Liu Y, Babarsky R, Swerdlin SP. 2010. A reanalysis system for the generation of mesoscale climat-ographies. *J. Appl. Meteorol. Climatol.* **49**: 954–972, doi: 10.1175/2009JAMC2351.1.

Hahmann AN, Vincent CL, Peña A, Lange J, Hasager CB. 2015. Wind climate estimation using WRF model output: Method and model sensitivities over the sea. *Int. J. Climatol.* **35**: 3422–3439, doi: 10.1002/joc.4217.

Kristensen L, Jensen NO. 1979. Lateral coherence in isotropic turbulence and in the natural wind. *Boundary Layer Meteorol.* **17**: 353–373, doi: 10.1007/BF00117924.

Larsén XG, Vincent C, Larsen S. 2013. Spectral structure of mesoscale winds over the water. *Q. J. R. Meteorol. Soc.* **139**: 685–700, doi: 10.1002/qj.2003.

Nanahara T, Asari M, Sato T, Yamaguchi K, Shibata M, Maejima T. 2004. Smoothing effects of distributed wind turbines. Part 1. Coherence and smoothing effects at a wind farm. *Wind Energy* **7**: 61–74, doi: 10.1002/we.109.

Peña Diaz A, Mikkelsen T, Gryning SE, Hasager CB, Hahmann AN, Badger M, Karagali I, Courtney M. 2012. *Offshore Vertical Wind Shear: Final Report on NORSEWInDs Work Task 3.1*. DTU Wind Energy: Roskilde, Denmark.

Reynolds RW, Smith TM, Liu C, Chelton DB, Casey KS, Schlax MG. 2007. Daily high-resolution-blended analyses for sea surface temperature. *J. Clim.* **20**: 5473–5496, doi: 10.1175/2007JCLI1824.1.

St. Martin CA, Lundquist JK, Handschy MA. 2015. Variability of interconnected wind plants: Correlation length and its dependence on variability time scale. *Environ. Res. Lett.* **10**: 044004, doi: 10.1088/1748-9326/10/4/044004.

Schlez W, Infield D. 1998. Horizontal, two point coherence for separations greater than the measurement height. *Boundary-Layer Meteorol.* **87**: 459–480, doi: 10.1023/A:1000997610233.

Skamarock WC. 2004. Evaluating mesoscale NWP models using kinetic energy spectra. *Mon. Weather Rev.* **132**: 3019–3032, doi: 10.1175/MWR2830.1.

Sørensen P, Hansen AD, Rosas PAC. 2002. Wind models for simulation of power fluctuations from wind farms. *J. Wind. Eng. Ind. Aerodyn.* **90**: 1381–1402, doi: 10.1016/S0167-6105.(02)00260-X .

Sørensen P, Cutululis NA, Vigueras-Rodríguez A, Madsen H, Pinson P, Jensen L, Hjerrild J, Donovan M. 2008. Modelling of power fluctuations from large offshore wind farms. *Wind Energy* **11**: 29–43, doi: 10.1002/we.246.

© 2016 The Authors. *Quarterly Journal of the Royal Meteorological Society* published by John Wiley & Sons Ltd on behalf of the Royal Meteorological Society.

Troldborg N, Larsen GC, Madsen HM, Hansen KS, Sørensen JN, Mikkelsen R. 2011. Numerical simulations of wake interaction between two wind turbines at various inflow conditions. *Wind Energy* **14**: 859–876, doi: 10.1002/we.433.

Vigueras-Rodríguez A, Sørensen P, Viedma A, Donovan MH, Gómez Lázaro E. 2012. Spectral coherence model for power fluctuations in a wind farm. *J. Wind Eng. Ind. Aerodyn.* **102**: 14–21, doi: 10.1016/j.jweia.2011.12.006.

Vincent CL, Hahmann AN. 2015. The impact of grid and spectral nudging on the variance of the near-surface wind speed. *J. Appl. Meteorol. Climatol.* **54**: 1021–1038, doi: 0.1175/JAMC-D-14-0047.1.

Vincent CL, Pinson P, Giebel G. 2011. Wind fluctuations over the North Sea. *Int. J. Climatol.* **31**: 1584–1595, doi: 10.1002/joc.2175.

Vincent CL, Larsén XG, Larsen SE, Sørensen P. 2013. Cross-spectra over the sea from observations and mesoscale modelling. *Boundary-Layer Meteorol.* **146**: 297–318, doi: 10.1007/s10546-012-9754-1.

Woods JW, Davy RJ, Russell CJ, Coppin PA. 2011. Cross-spectrum of wind speed for meso-gamma scales in the upper surface layer over southeastern Australia. *Boundary-Layer Meteorol.* **141**: 93–116, doi: 10.1007/s10546-011-9632-2.

© 2016 The Authors. *Quarterly Journal of the Royal Meteorological Society* published by John Wiley & Sons Ltd on behalf of the Royal Meteorological Society.